Smart Structures and Systems, *Vol. 31, No. 3 (2023) 259-273*
https://doi.org/10.12989/sss.2023.31.3.259

Validation of model-based adaptive control method for real-time hybrid simulation

Xizhan Ning [1,2a], Wei Huang [1b], Guoshan Xu[*3], Zhen Wang [4c] and Lichang Zheng [3d]

[1] *College of Civil Engineering, Huaqiao University, Xiamen 361021, China*
[2] *Key Laboratory for Intelligent Infrastructure and Monitoring of Fujian Province, Huaqiao University, Xiamen 361021, China*
[3] *School of Civil Engineering, Harbin Institute of Technology, Harbin 150090, China*
[4] *School of Civil Engineering and Architecture, Wuhan University of Technology, Wuhan 430070, China*

(*Received July 23, 2022, Revised November 28, 2022, Accepted March 21, 2023*)

Abstract. Real-time hybrid simulation (RTHS) is an effective experimental technique for structural dynamic assessment. However, time delay causes displacement de-synchronization at the interface between the numerical and physical substructures, negatively affecting the accuracy and stability of RTHS. To this end, the authors have proposed a model-based adaptive control strategy with a Kalman filter (MAC-KF). In the proposed method, the time delay is mainly mitigated by a parameterized feedforward controller, which is designed using the discrete inverse model of the control plant and adjusted using the KF based on the displacement command and measurement. A feedback controller is employed to improve the robustness of the controller. The objective of this study is to further validate the power of dealing with a nonlinear control plant and to investigate the potential challenges of the proposed method through actual experiments. In particular, the effect of the order of the feedforward controller on tracking performance was numerically investigated using a nonlinear control plant; a series of actual RTHS of a frame structure equipped with a magnetorheological damper was performed using the proposed method. The findings reveal significant improvement in tracking accuracy, demonstrating that the proposed method effectively suppresses the time delay in RTHS. In addition, the parameters of the control plant are timely updated, indicating that it is feasible to estimate the control plant parameter by KF. The order of the feedforward controller has a limited effect on the control performance of the MAC-KF method, and the feedback controller is beneficial to promote the accuracy of RTHS.

Keywords: feedforward and feedback; Kalman filter; model-based adaptive control; real time hybrid simulation

1. Introduction

Real-time hybrid simulation (RTHS) (Nakashima *et al*. 1992) is an innovative and promising test technique in structural seismic engineering. In contrast to other test methods, it can not only reproduce structural response under earthquake excitation but can also overcome practical problems caused by test location and costs (Horiuchi *et al*. 1999, Blakeborough *et al*. 2001, Chen *et al*. 2019). This technique, derived from pseudo-dynamic testing (Hakuno *et al*. 1969) (also called hybrid simulation), splits the emulated structure into two parts. The part with a clear constitutive model is generally regarded as the numerical substructure (NS), which is simulated by computer programs. The rest part is regarded as the physical substructure (PS) and is loaded in a laboratory. The boundary condition between these two substructures is realized by an actuator or shaking table (Mukai *et al*. 2020). In RTHS, the displacement calculated by the equation of motion is imposed on the PS via loading devices, and then the measured restoring force is fed back to the NS for displacement calculation at the next time step (McCrum and Williams 2016, Al-Subaihawi *et al*. 2022). Nowadays, some new progresses have been made in RTHS considering structural or external excitation uncertainties (Tsokanas *et al*. 2021, Chen *et al*. 2022, Gao *et al*. 2022, Xu *et al*. 2022). However, the key to a successful RTHS is that the above procedures must be completed accurately in real time (Mirza Hessabi *et al*. 2016, Fermandois and Quiroz 2021).

In the experimental process, certain factors, such as the dynamics of servo-hydraulic actuators and physical specimens, data transmission, and noise, inevitably cause displacement de-synchronization between the NS and PS. Generally, this phenomenon is known as time delay, resulting in inaccurate results and experimental instability (Darby *et al*. 2002, Maghareh *et al*. 2014, Huang *et al*. 2019, Chen and Chen 2020).

To reduce the negative effect of the time delay, time delay compensation or control strategies have been proposed in the development course of RTHS. Based on the assumption of constant time delay, polynomial extrapolation (Horiuchi *et al*. 1999) and kinematic predict method (Horiuchi and Konno 2001) were first proposed and validated, among which the polynomial extrapolation is the most popular method. Then, classical control theories were

*Corresponding author, Associate Professor,
E-mail: xuguoshan@hit.edu.cn
[a] Associate Professor, E-mail: xzning@hqu.edu.cn
[b] Graduate Student, E-mail: huang_wei1996@163.com
[c] Professor, E-mail: wang_zhen@whut.edu.cn
[d] Ph.D. Candidate, E-mail: 21b933054@stu.hit.edu.cn

ISSN: 1738-1584 (Print), 1738-1991 (Online)

also adopted and improved to solve the time delay problem in RTHS, such as phase-lead control (Zhao *et al*. 2003), feedforward control (Hayati and Song 2017), and inverse control (Chen and Ricles 2009). Recently, various attempts have been made to use the modern control theories in designing the tracking controller for RTHS, i.e., model-based control (Carrion and Spencer 2008, Phillips and Spencer 2013, Nakata and Stehman 2014), robust control (Ou *et al*. 2015), and sliding mode control (Condori *et al*. 2020, Li *et al*. 2022). The above methods have been numerically and/or experimentally examined.

However, due to the dynamics of loading systems and PS, time delay in RTHS exhibits time-varying characteristics. To deal with the variable time delay, adaptive strategies, combining system identification and parameter updating, have got a broad concern, such as the adaptive inverse control method (Strano and Terzo 2016, Simpson *et al*. 2020), adaptive time series (ATS) method based on actuator model (Chae *et al*. 2013) and its improvement, conditional ATS (Palacio-Betancur and Gutierrez Soto 2019), physical testing system model based adaptive strategies (Wang *et al*. 2020), adaptive model predictive method (Tsokanas *et al*. 2022), and adaptive model-based control method (Najafi and Spencer 2019, Gálmez and Fermandois 2022). Additionally, the novel adaptive control methods integrating with two kinds of different control theories have exhibited outstanding tracking performance, such as the robust model predictive control combining polynomial extrapolation and model prediction (Tsokanas *et al*. 2020), and the passivity control with adaptive feed-forward filtering (Peiris *et al*. 2020). Recently, Ning *et al*. (2022) proposed a model-based adaptive control strategy with KF (MAC-KF), whose control accuracy was verified through numerical simulations.

To further validate the effectiveness and feasibility of the MAC-KF method, numerical simulations utilizing a nonlinear control plant and actual experiments are performed in this study. In particularly, the effect of the order of the feedforward controller and the feedback controller on tracking performance is investigated. This study is a supplement and improvement of the companion work. This paper is mainly organized as follows. Section 2 briefly describes the overview of MAC-KF. The numerical validation using the nonlinear control plant is presented in Section 3, including the introduction of the nonlinear control plant, controller design, and result discussion. Section 4 mainly illustrates the experimental verification results. Section 5 concludes the study.

2. Overview of model-based adaptive control method with KF

The block diaphragm of a typical RTHS is shown in Fig. 1, where the emulated structure is split into NS and PS. To realize high accuracy and enhance the stability of RTHS, an adaptive model-based control method with a KF was developed, as presented in Fig. 1(c). As shown in the figure, the proposed control method consists of a feedforward controller with adjustable parameters, a parameter estimator adopting a KF, and a feedback controller.

In the proposed method, the servo-hydraulic actuator, along with the PS, is regarded as a unit and termed as control plant. It can be represented by a rational proper transfer function without zeros. Hence, the relationship between the commanded and measured displacements can be expressed as

$$d_{\mathrm{m}} = G_s(s)d_{\mathrm{c}} = \frac{1}{a_n s^n + a_{n-1}s^{n-1} + \ldots + a_1 s + a_0} d_{\mathrm{c}} \tag{1}$$

where s represents the Laplace operator, n denotes the order of the transfer function, $a_0, a_1, \ldots, a_n$ represent the coefficients of the denominator, and d_{c} and d_{m} represent the commanded and measured displacements, respectively. In the proposed method, an inverse model is used to generate the commanded displacement using the desired displacement d. The feedforward controller can be expressed as

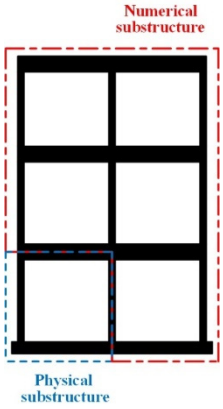

(a) Partitioning of substructures

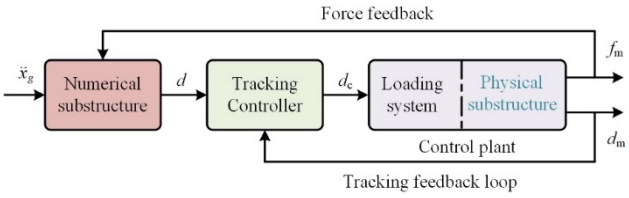

(b) Flowchart of typical RTHS

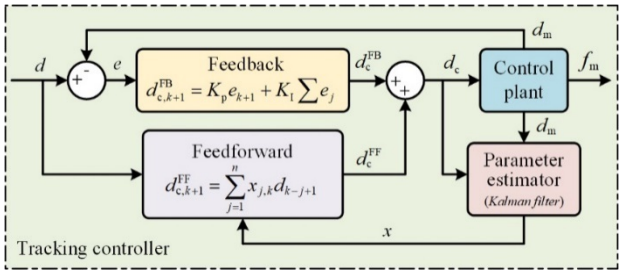

(c) Schematic of MAC-KF

Fig. 1 Block diagram of typical RTHS

$$d_c = G_s^{-1}(s)d = (a_n s^n + a_{n-1}s^{n-1} + \ldots + a_1 s + a_0)d = a_n d^{(n)} + a_{n-1} d^{(n-1)} + \ldots + a_1 d^{(1)} + a_0 d \quad (2)$$

Because responses obtained by Eq. (2) typically differ from the actual ones, the feedforward controller does not perform as expected. Hence, it is necessary to identify the transfer function of the control plant and calculate the parameters $a_0, a_1, \ldots, a_n$ in real time. For practical convenience, the difference equation is introduced into Eq. (2); thus, a discrete-time feedforward controller can be obtained as

$$d_{c,k}^{FF} = x_{1,k}d_k + x_{2,k}d_{k-1} + \ldots + x_{q,k}d_{k-q+1} = \sum_{j=1}^{q} x_{j,k}d_{k-j+1} \quad (3)$$

where $x_1, x_2, \ldots, x_q$ represent control plant parameters related to the parameters $a_0, a_1, \ldots, a_n$ and the discrete-time interval Δt, and $d_{c,k}^{FF}$ and d_k denote the commanded displacement provided by the feedforward controller and the desired displacements at the k^{th} step, respectively. By applying the feedforward controller, the measured displacement is identical to the desired displacement in an ideal situation, making it possible to replace d in Eq. (2) or Eq. (3) with d_m. Thus, the commanded displacement d_c and measured displacement d_m can be used to estimate x.

Let vector $\mathbf{x} = [x_1, x_2, \ldots, x_q]^T$; under the assumption of slowly changed control plant parameters, the following state-space equations can be obtained

$$\mathbf{x}_{k+1} = \mathbf{x}_k \quad (4)$$

$$d_{c,k} = \mathbf{H}_k \mathbf{x}_k + v_k \quad (5)$$

where $\mathbf{H}_k = [d_{m,k}, d_{m,k-1}, \ldots, d_{m,k-q+1}]$ and v represents the measurement noise that satisfies

$$\mathbf{E}v_k = 0, \quad \mathbf{E}v_k v_k^T = R \quad (6)$$

where R represents the measurement noise covariance.

Eqs. (4) and (5) show that it is a linear estimation problem when using the measured displacement to estimate the control plant parameters. Hence, the KF is employed in the proposed method, whose formulas are concisely given below

$$\hat{\mathbf{x}}_{k+1} = \hat{\mathbf{x}}_k + \mathbf{K}_k(d_{m,k} - \mathbf{H}_k\hat{\mathbf{x}}_k) \quad (7)$$

$$\mathbf{K}_k = \mathbf{P}_{k-1}\mathbf{H}_k^T(\mathbf{H}_k\mathbf{P}_{k-1}\mathbf{H}_k^T + R)^{-1} \quad (8)$$

$$\mathbf{P}_k = (\mathbf{I} - \mathbf{K}_k\mathbf{H}_k)\mathbf{P}_{k-1} \quad (9)$$

where $\hat{\mathbf{x}}$ represents the estimate of $\mathbf{x}$, $\mathbf{K}$ and $\mathbf{P}$ denote the Kalman gain and the estimate error covariance, respectively, and $\mathbf{I}$ represent a unit matrix with respect to the number of parameters.

3. Numerical validation with nonlinear control plant model

Numerical investigations employing a linear actuator model have been carried out by Ning *et al*. (2022), and the proposed method exhibits excellent tracking performance and strong robustness. However, considering that the testing system and PS will be influenced by different degrees of nonlinearity in real applications, numerical validations using a nonlinear control plant model are presented and discussed in this section. Three criteria in the benchmark problem (Silva *et al*. 2020), namely, the calculated time delay J_1, the normalized root mean square of the tracking error J_2, and the peak tracking error J_3, are adopted to evaluate control performance, which are defined by

$$J_1 = \arg\max_h \left(\sum_k d_k d_{m,k-h} \right) \quad (10)$$

$$J_2 = \sqrt{\frac{\sum_{k=1}^{j} (d_k - d_{m,k})^2}{\sum_{k=1}^{j} (d_k)^2}} \times 100\% \quad (11)$$

$$J_3 = \frac{\max|d_k - d_{m,k}|}{\max|d_k|} \times 100\% \quad (12)$$

where j denotes the number of data points, and d and d_m denote the desired displacement and the measured displacement, respectively.

3.1 Reference structure model

The evaluated structure is a three-story steel structure with a magnetorheological (MR) damper, as shown in Fig. 2. The PS, namely, the MR damper, is installed between the first floor and the ground. For convenience, the MR damper and actuator are regarded as a unit and termed a nonlinear control plant. Assuming that the flexural stiffness of beams is infinite, the dynamic model of the structure can be simplified to the story shear model, and only the horizontal degree of freedom is considered for each story. The mass and stiffness matrixes of the structure are expressed in Eqs. (13) and (14), respectively, resulting in natural frequencies of 3.04, 8.51, and 12.30 Hz, respectively.

$$\mathrm{M} = \begin{bmatrix} 20.5 & 0 & 0 \\ 0 & 20.5 & 0 \\ 0 & 0 & 20.5 \end{bmatrix} \times 10^3 \text{ kg} \quad (13)$$

$$K = \begin{bmatrix} 7.5460 & -3.7730 & 0 \\ -3.7730 & 7.5460 & -3.7730 \\ 0 & -3.7730 & 3.7730 \end{bmatrix} \times 10^7 \text{ N/m} \quad (14)$$

Adopting the Rayleigh damping assumption with the first and the second damping ratio of 2%, the structural damping matrix can be written in Eq. (15).

In this section, the El Centro (1940, NS) with peak ground acceleration (PGA) scaled to 0.25 g was selected as the structural excitation for numerical validation. The central difference algorithm was adopted to solve the equation of motion with a time interval of 1/1024 s.

$$C = \begin{bmatrix} 7.9680 & -3.1186 & 0 \\ -3.1186 & 7.9680 & -3.1186 \\ 0 & -3.1186 & 4.8494 \end{bmatrix} \times 10^4 \text{ N·s/m} \quad (15)$$

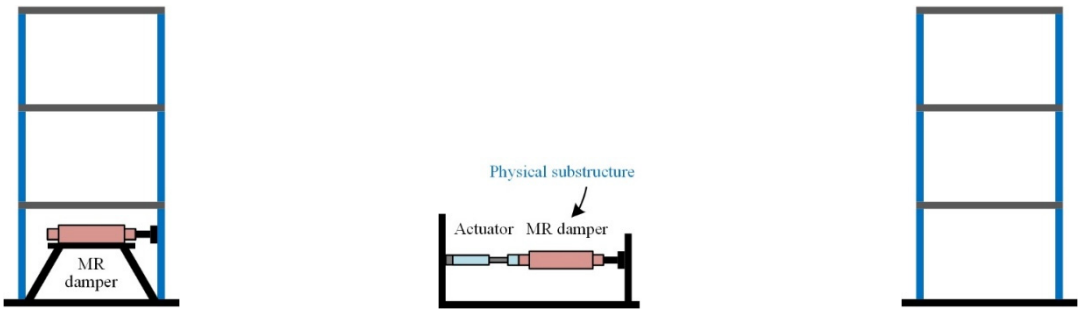

(a) Reference structure (b) Nonlinear control plant (c) Numerical substructure

Fig. 2 Structure model

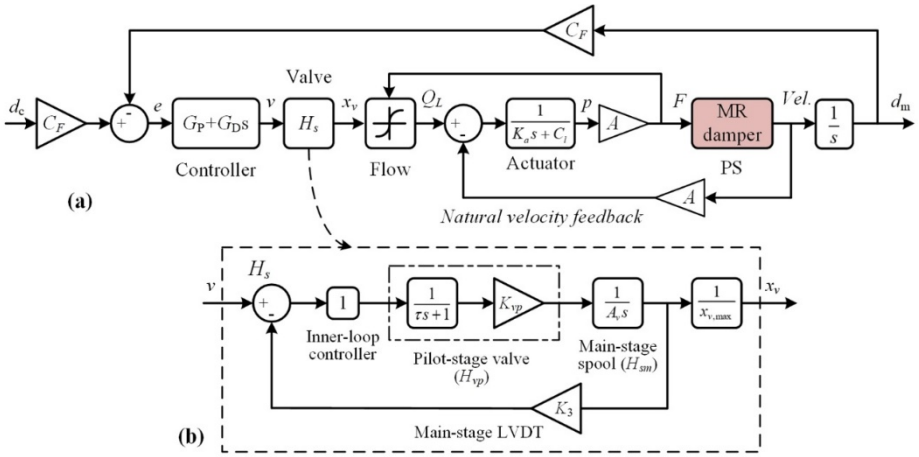

Fig. 3 Block diaphragm of nonlinear control plant

3.2 Overview of the nonlinear control plant

The servo-hydraulic actuator system provided by Zhao *et al*. (2005). is adopted in this study, as shown in Fig. 3. The nonlinear actuator model is mainly composed of an actuator and its servo-valve, with the natural velocity feedback considered. The model can account for the effects of nonlinear factors in RHTS, including the flow property, response delay of the servo-valve, and the interaction between the PS and actuator. For brevity, the principle of the actuator is excluded, with the symbols described in Table 1. The PS, namely, the MR damper in Fig. 3, is represented by the Bouc-Wen model proposed by Weber (2013), which can be expressed as

$$f_{\mathrm{m}}(i) = \alpha(i)z + c(i)\dot{x}_d \tag{16}$$

$$z = C\dot{x}_{\mathrm{d}} - \beta\dot{x}_{\mathrm{d}}|z|^{\theta} - \gamma|\dot{x}_{\mathrm{d}}|z|\dot{z}|^{\theta\text{-}1} \tag{17}$$

$$\alpha(i) = \alpha_{\mathrm{a}} + \alpha_{\mathrm{b}}(i - 1.2i_{\max})^2 \tag{18}$$

$$c(i) = c_{\mathrm{a}} + c_{\mathrm{b}}i \tag{19}$$

where $\alpha(i)$ and the viscous coefficient $c(i)$ are functions related to the input current i in the MR damper; $\dot{x}_{\mathrm{d}}$ is veolocity of the damper; the C, β, γ, and θ denote the shape parameters of the hysteretic loop; $i_{\max}$ represents the maximum MR damper current; α_{a} and α_{b} denote the shaping parameters in the function $\alpha(i)$; c_{a} and c_{b} denote the intercept and slope of the function $c(i)$, respectively. All parameters and their definitions in the nonlinear control plant are listed in Table 1.

3.3 Controller design

In the companion study, it is revealed that the initial settings of the KF and feedback controller have a limited effect on the proposed method, where the feedforward controller was designed using a second-order transfer function (namely, a three-parameter feedforward controller). As a supplement, the effect of the order of the feedforward controller is studied in this subsection. Three different feedforward controllers, namely, two-, three-, and four-parameter feedforward controllers, are considered, corresponding to MAC-KF(2), MAC-KF(3), and MAC-KF(4) in Table 2, respectively. In addition, adaptive delay compensation (ADC) based on KF without feedback controller is also considered in this study. Similar to MAC-KF method, the two-, three- and four-parameter feedforward controllers are employed, referred to ADC-KF(2), ADC-KF(3), and ADC-KF(4), respectively. Preliminary simulation was performed using an uncontrolled control plant, where the displacement command was a swept signal with an amplitude of 5 mm and a frequency range from 0.1 to 10 Hz. The duration of this simulation was 60 s. Then, the commanded and

measured displacements obtained from this simulation were used to calculate the initial parameters $\mathbf{x}_0$ by the least square method, as listed in Table 2. For all control methods presented in this table, the initial estimate error covariance $\mathbf{P}_0$ and the measurement noise covariance R are set to diag[$(\mathbf{x}_0)^2$] and 10^{-4}, respectively.

Table 1 Parameter values of nonlinear control plant (Zhao *et al*. 2005, Weber 2013)

Parameter	Description	Value	Unit
C_F	Conversion factor	78.4	V/m
G_P	Proportional gain	3	-
G_D	Derivative gain	0	-
$x_{v\,max}$	Maximum spool stroke	2.79×10^{-3}	m
K_{vp}	Sensitivity factor	1.06×10^{-5}	$m^3/s/V$
τ_{vp}	Valve flow gain	0.0014	s
A_v	Equivalent time constant	1.964×10^{-4}	m^2
K_3	Main-stage spool area	3579.13	V/m
K_v	Flow gain	1.64×10^{-2}	m^3/s
p_s	Pressure supply	1.9×10^4	kPa
C_l	Leakage coefficient	1.3×10^{-8}	$m^3/s/ksi$
K_a	Compressibility coefficient	7.56×10^{-10}	m^3/kPa
A	Actuator piston area	8.212×10^{-3}	m^2
γ	Parameters associated with the hysteretic loop	200	m^{-1}
β		200	m^{-1}
θ		2	-
C		5000	m^{-1}
α_a	Shaping parameters	4250	N
α_b		−27.78	N/A^2
c_a	Parameters related to the viscous coefficient	1400	Ns/m
c_b		1000	Ns/m/A

A series of simulations were carried out with the designed feedforward controller, and a sinusoidal signal with an amplitude of 5 mm and a frequency of 2 Hz served as the commanded displacement. Each simulation lasted 60 s. A total of 30 simulations with different PI gains were performed to determine the optimal PI value, and J_2 and J_3 are shown in Fig. 4. Note that the results of J_1 are not presented in this figure because its values are all 0 ms in all PI gain combinations.

As shown in Fig. 4, with an increase in K_P, J_2 and J_3 first decrease and then gradually increase. For a given K_P, J_2 and J_3 remain almost constant as K_I varies from 0 to 5. This demonstrates that K_P obviously affects the performance of the three MAC-KF methods, whereas the influence of K_I can be neglected. Moreover, when K_P = 4, 6, or 8, J_2 and J_3 exhibit no remarkable change even though the number of parameters in the feedforward controller varies from 2 to 4. This shows that these K_P settings can make the MAC-KF method remain relatively stable. Hence, the optimal PI gain combination is set as K_P = 6 and K_I = 0.

3.4 Results analysis

To evaluate the superiority of the proposed MAC-KF control method, this subsection presents the virtual RTHS (vRTHS) results of seven simulations under El Centro seismic excitation, including a simulation for the control plant without any control method and six simulations generated with different control methods. In all simulations, the PGA of seismic excitation was scaled to 0.25 g.

The results of J_1 to J_3 for seven simulations are listed in Table 3. In the table, "Bare" denotes the simulation for the control plant without any control measure. As shown in the

Table 2 Controller parameter settings for six methods

Number	Method	Description	K_P	K_I	Initial parameters $\mathbf{x}_0$
1	ADC-KF(2)	Two-parameter feedforward, without feedback	-	-	[1.2811; -0.6793]
2	ADC-KF(3)	Three-parameter feedforward, without feedback			[1.5603; -1.1341; 0.4863]
3	ADC-KF(4)	Four-parameter feedforward, without feedback			[1.7901; -1.5776; 0.9905; -0.3976]
4	MAC-KF(2)	Two-parameter feedforward, with feedback	6	0	[1.2811; -0.6793]
5	MAC-KF(3)	Three-parameter feedforward, with feedback			[1.5603; -1.1341; 0.4863]
6	MAC-KF(4)	Four-parameter feedforward, with feedback			[1.7901; -1.5776; 0.9905; -0.3976]

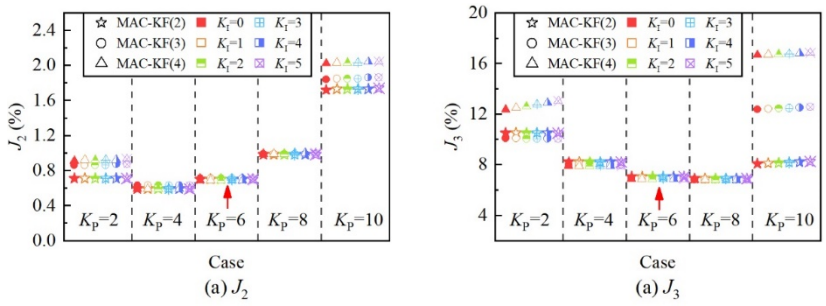

Fig. 4 J_2 and J_3 in 30 PI gain combinations

Table 3 RTHS evaluation criteria for seven simulations

Number	Method	J_1 (ms)	J_2 (%)	J_3 (%)
1	ADC-KF(2)	2	5.80	9.21
2	ADC-KF(3)	2	4.90	5.82
3	ADC-KF(4)	2	4.76	7.05
4	MAC-KF(2)	0	1.56	1.85
5	MAC-KF(3)	0	1.49	1.37
6	MAC-KF(4)	0	1.47	1.70
7	Bare	21.50	38.27	35.23

table, the evaluation criteria of methods 1-6 reduced significantly compared with those of "Bare." This demonstrates that the MAC-KF control methods can effectually reduce the time delay in RTHS and have excellent tracking performance, regardless of whether a PI feedback controller is added. According to the results of methods 1-3, as the number of feedforward controller parameters increases from 2 to 4, J_2 decreases gradually. When the number of parameters was varied, J_1 remained unchanged, whereas J_3 first decreased significantly and then increased continuously. Similar conclusions can be generated from the results of methods 4-6. When the same feedforward controller parameter settings were guaranteed, the method equipped with PI feedback can reduce the evaluation criteria compared with those without PI: J_1 decreases from 2 to 0 ms; the maximum decrease in J_2 and J_3 is 73.10% ((5.80−1.56)/5.80) and 79.91% ((9.21 − 1.85) / 9.21), respectively.

The displacement time histories for methods 1-6 are investigated. Owing to the almost perfect agreement between the desired and measured displacements, the global displacement time histories are omitted, and only the enlarged views for each method are presented, as shown in Fig. 5, with the views at zero and peak displacement for the same time provided in each subfigure. In the figure, "Desired" and "Measured" denote the desired and measured displacements, respectively. For instance, "Deisred_1" denotes the desired displacement of method 1 in vRTHS. The displacement time histories of method 7 are not shown in Fig. 5 because the evaluation criteria of this situation are the worst.

It is seen in Figs. 5(a)-(c) that there are obvious displacement discrepancies between the desired and measured displacements for methods 1 to 3, whether at zero or peak displacement. With the increase of the number of controller parameters, the discrepancies at peak displacement decrease gradually, while that of zero displacements are negligible, indicating that the ADC-KF methods are susceptible to the feedforward controller structure. Conversely, the displacement discrepancies for methods 4 to 6 are reduced at both zero and peak displacements, and "Measured_4" to "Measured_6" can better match their corresponding desired displacements, as presented in Figs. 5(d)-(f). For methods 1-3, the displacement agreements between the desired and measured displacements are lower than those of methods 4-6, demonstrating that the MAC-KF method can significantly reduce the time delay and tracking error in RTHS. Furthermore, owing to the addition of feedback control, the MAC-KF's performance did not vary significantly with the change in the number of controller parameters, indicating strong stability of the MAC-KF.

Fig. 6 plots the contrastive estimated parameter time

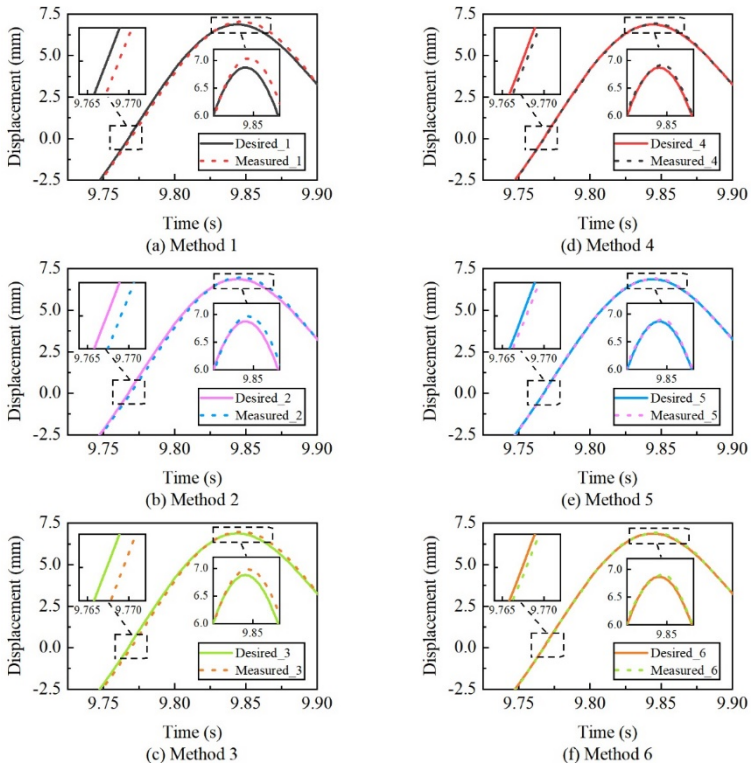

Fig. 5 Enlarged view of displacement time histories for methods 1-6

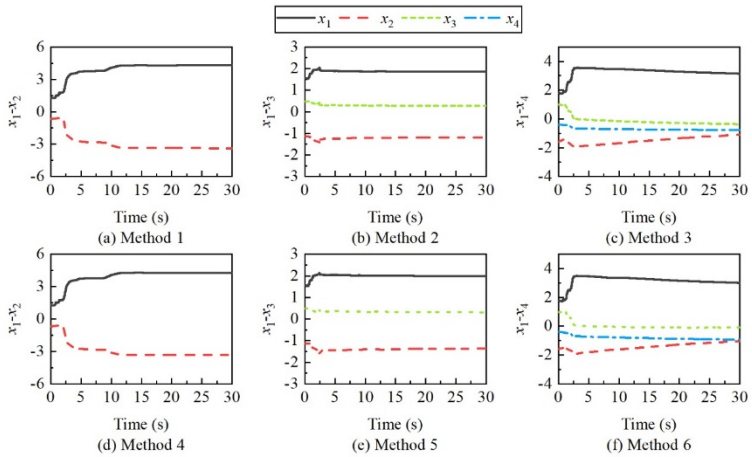

Fig. 6 Estimated parameter time histories for methods 1-6 in vRTHS

histories for methods 1-6 in vRTHS. It can be seen that the controller parameters of the six methods start to update at the beginning of vRTHS, but the variation ranges are very small. With the increase of the commanded displacement, the nonlinearity of the control system develops, resulting in the estimated parameters change rapidly in the following 2 s. Then, the estimated parameters fluctuate in a relatively small range. The reason can be interpreted as follows. The time delay of the system is large at the beginning, and the initial parameters are different from the actual ones. To track the commanded displacement, the parameters must be adjusted quickly, and then the primary time delay is compensated effectively by the adaptive controller using the updated parameters. However, the time delay cannot be eliminated due to the time-varying nonlinearities of the system. The parameters must be adjusted continuously to remedy the residual time delay, resulting in a small variation in the later stage.

By comparing the estimation results of controllers with the same structure, it is found that the evolutions of the estimated parameter varied consistent. If focusing on MAC-KF or ADC-KF, it can be seen that the estimated parameters of two-parameter controllers have a significantly varying range for the first 10 s. While for three- and four-parameter controllers, the fluctuation ranges are relatively small. The reason is that the two-parameter system model cannot accurately represent the dynamic characteristics of the control plant. To track the displacement command, the parameters in the controller must be adjusted consecutively using the measured displacement, which in turn leads to the long parameter change duration.

4. Experimental validation

4.1 Experimental setup

To further investigate the performance of the proposed method and explore the possible challenges in actual experiments, RTHS was carried out at the Structural and Seismic Testing Center, Harbin Institute of Technology. The target structure is a moment-resisting steel frame structure

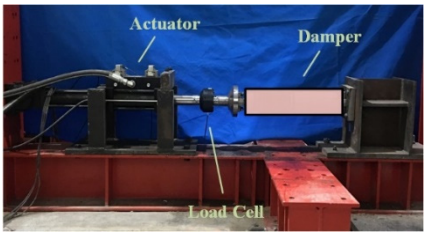

Fig. 7 Experimental setup

with a damper installed between the first floor and the ground, which is identical to the structure used in Section 3. The damper is taken as the PS and tested in the laboratory. Fig. 7 shows the experimental setup. The testing system consists of a hydraulic actuator and dSPACE. The former is controlled by the MTS793 software and a Flex Test GT60 Controller, and the maximum values of the dynamic displacement and force are ±125 mm and 100 kN, respectively. The latter is composed of a DS1103 card and ControlDesk software. The two parts are connected by BNC lines. In the RTHS, the proposed controller and the stepwise integration method are modeled with MATLAB/Simulink and then compiled and ran on dSPACE.

4.2 Controller design

Similar to the description in Section 3.3, the initial parameters and the optimal PI gain combination in the control methods were determined by swept and sine signals, respectively. The initial parameters $\mathbf{x}_0$ were calculated by the least squares method. Considering the maximum range of the servo actuator and the oscillation phenomenon in the hybrid tests, 10 combinations in Table 4 were employed to set the optimal PI gain combination. The obtained J_2 and J_3 are shown in Fig. 8. Specifically, the J_2 values of methods 4-6 are presented in Figs. 8(a)-(c), respectively, and Figs. 8(d)-(f) list the J_3 values of methods 4-6, respectively. Note that the values of J_1 remained constant at 0 ms; hence, they are not shown in Fig. 8.

As shown in Figs. 8(a)-(c), the values of J_2 for Combinations 1-5 are relatively small in all cases.

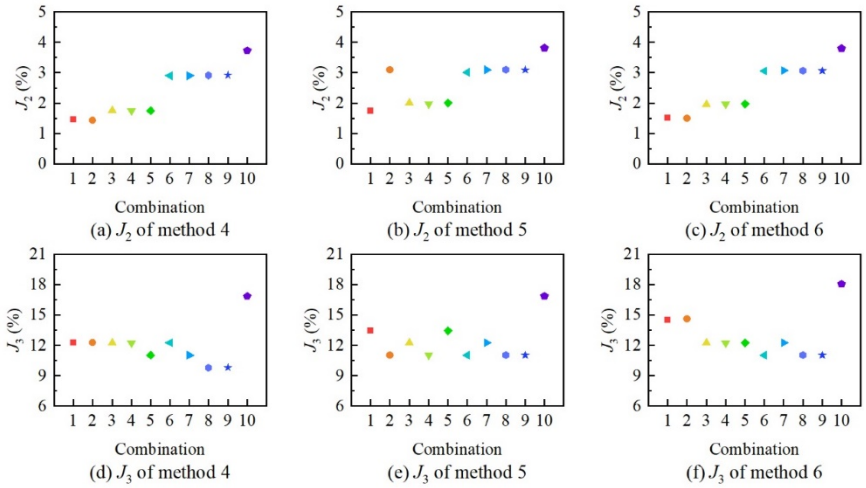

Fig. 8 J_2 and J_3 of methods 4-6 under 10 PI gain combinations

Table 4 PI gain parameter settings for various kinds of MAC-KF methods in RTHS

Combination	K_P	K_I
1	0.2	0
2		0.1
3	0.5	0
4		0.1
5		0.2
6	1.0	0
7		0.1
8		0.2
9		0.5
10	1.5	0

Therefore, Combinations 1-5 were selected as candidates for the optimal PI gain combination. As shown in Fig. 8(d), the value of J_3 for Combination 5 was the smallest among all alternatives. Thus, the optimal case of MAC-KF(2) was set as Combination 5: K_P = 0.5 and K_I = 0.2. In Fig. 8(e), the value of J_3 for Combinations 2 and 4 both satisfied the optimal requirement, whereas Combination 2 had a larger J_2. Hence, Combination 4 was selected as the optimal PI combination of MAC-KF(3). Moreover, synthetically considering the J_2 and J_3 in Figs. 8(c) and 8(f), Combination 1 was selected as the optimal PI gain combination of MAC-KF(4). The initial parameter and the optimal PI gain combination for methods 1-6 are listed in Table 5. For other parameters, the initial estimate error covariance $\mathbf{P}_0$ = diag $[(x_0)^2]$, and the measurement noise covariance R is 10^{-4}.

4.3 Assessment of control accuracy with prescribed displacement commands

This subsection assesses the control accuracy of six methods under a prescribed displacement command. The displacement command is a 0.1-3 Hz swept signal, which has an amplitude of 5 mm and a duration of 100 s. The

Table 5 Parameter settings for six methods in RTHS

Number	Method	K_P	K_I	Initial parameters $\mathbf{x}_0$
1	ADC-KF(2)	-	-	[2.9038; -2.2546]
2	ADC-KF(3)			[2.2477; -1.0034; -0.6564]
3	ADC-KF(4)			[2.4456; -2.7503; 2.1531; -1.3700]
4	MAC-KF(2)	0.5	0.2	[2.9038; -2.2546]
5	MAC-KF(3)	0.5	0.1	[2.2477; -1.0034; -0.6564]
6	MAC-KF(4)	0.2	0	[2.4456; -2.7503; 2.1531; -1.3700]

Table 6 Values of J_1-J_3 for methods 1-6 under 3Hz swept signal

Number	Method	J_1 (ms)	J_2 (%)	J_3 (%)
1	ADC-KF(2)	1	2.22	5.92
2	ADC-KF(3)	1	2.50	7.06
3	ADC-KF(4)	1	2.42	7.50
4	MAC-KF(2)	0	2.14	5.33
5	MAC-KF(3)	0	2.27	5.57
6	MAC-KF(4)	0	2.22	6.69

obtained evaluation criteria are listed in Table 6. The following phenomena can be found from methods 1-3: (i) the values of J_1 remained at 1 ms, and there were no variations; (ii) the values of J_2 are less than 2.5%; (iii) the values of J_3 increase gradually as the order of the feedforward controller increases. Similar conclusions can be achieved for methods 4-6. As presented in Table 6, the values of J_2 are almost the same for methods 1-6. However, the values of J_1-J_3 provided by methods 4-6 were smaller than those by methods 1-3.

The absolute values of displacement error between d and d_m for methods 1-6 under the swept signal are presented in Fig. 9. Figs. 9(a)-(c) show that the displacement errors of methods 1-3 are less than 0.2 mm in the first 40 s, and then

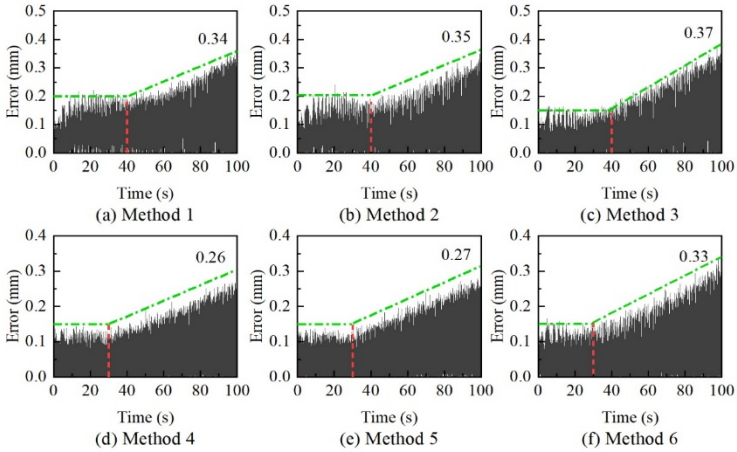

Fig. 9 Time histories of displacement error for methods 1-6 under 3-Hz swept signa

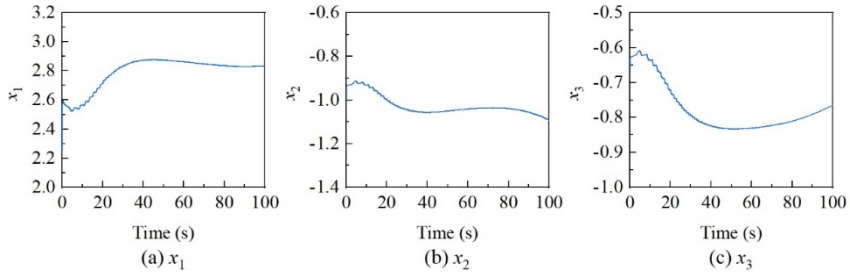

Fig. 10 Time histories of the estimated parameter for method 5 under swept signal

they gradually increase and finally reach the maximum values.

Moreover, when the number of parameters of the feedforward controller varies from 2 to 4, the maximum displacement errors gradually increase from 0.34 to 0.37 mm. Similar conclusions can be drawn from Figs. 9(d)-(f): the maximum displacement error of methods 4-6 also increases gradually as the number of parameters of the feedforward controller increases. The difference is that the displacement error of methods 4-6 begins to increase gradually after 30 s. Moreover, methods 4-6 have smaller displacement errors than methods 1-3. Based on the analysis of Table 6 and Fig. 9, the following conclusions can be drawn: (i) the feedback controller can improve the control performance of the proposed method, leading to fewer errors; (ii) an increase in the number of parameters of the feedforward controller cannot significantly improve the performance of the proposed method.

The time histories of the estimated parameter for method 5 under the swept signal are illustrated in Fig. 10. In the figure, the parameters are updated immediately as soon as the test begins. x_1-x_3 present relatively quick adaption from 0 s to approximately 40 s. Afterward, the parameters gradually changed, ultimately exhibiting no evident convergence. The main reason for this fact is that, under the swept signal, the control plant was negatively affected by different nonlinearities, resulting in a significant variation in time delay. To track the commanded displacement, the control plant parameters must be adjusted correspondingly.

4.4 Results of RTHS

To evaluate the control performance of the proposed MAC-KF methods used in RTHS, three seismic excitations were selected: (i) El Centro; (ii) Kobe; (iii) Morgan. The PGA was scaled to 0.10, 0.15, 0.20, and 0.25 g for each earthquake excitation. Here, the hybrid tests without a control strategy were also carried out to reflect the superiority of the proposed control method. For brevity, the evaluation criteria of methods 1-7 under 0.10-0.25 g are presented in Appendixes 1-4, and only the mean values are listed in Table 7. The evaluation criteria were calculated using the results of RTHS with different control methods under three earthquake acceleration values. In the table, "Bare" denotes hybrid testing without any control method.

Regarding method 7, the values of J_1 exceed 10 ms, and the values of J_2 and J_3 remain at the largest values. This is mainly because RTHS without any control strategy results in the accumulation of errors, further degrading the test accuracy. Compared with the "Bare" results, the evaluation criteria obtained from methods 1-6 are reduced: the values of J_1 are less than 3 ms in most cases, and the values of J_2 and J_3 are also less than 10%, indicating that the proposed method has excellent time-delay control ability and tracking performance.

The values of J_1-J_3 for methods 1-6 are shown in Fig. 11. Regarding methods 1-3, the values of J_1-J_3 decrease. This means that, for the control strategy without feedback control, excellent tracking performance can be achieved using a higher-order feedforward controller. According to

Table 7 Mean values of evaluation criteria for RTHS

Number	Method	Earthquake record	J_1 (ms)	J_2 (%)	J_3 (%)
1	ADC-KF(2)	El Centro	2.23	5.82	5.75
		Kobe	3.18	9.17	8.25
		Morgan	2.70	7.63	6.66
2	ADC-KF(3)	El Centro	2.23	5.71	5.72
		Kobe	2.70	8.67	7.56
		Morgan	2.70	7.45	6.86
3	ADC-KF(4)	El Centro	1.50	5.68	6.07
		Kobe	2.23	8.34	7.26
		Morgan	1.75	7.14	6.30
4	MAC-KF(2)	El Centro	0.00	4.35	4.51
		Kobe	0.25	6.77	5.06
		Morgan	0.25	5.89	5.32
5	MAC-KF(3)	El Centro	0.00	4.26	4.51
		Kobe	0.25	6.63	4.89
		Morgan	0.25	5.72	5.32
6	MAC-KF(4)	El Centro	0.25	4.49	5.18
		Kobe	0.75	7.16	5.97
		Morgan	0.50	6.10	5.07
7	Bare	El Centro	13.93	26.52	31.10
		Kobe	14.38	25.82	23.95
		Morgan	13.93	25.66	31.88

the results of methods 4-6, the following phenomena can be drawn: (i) for the same excitation, methods 4 and 5 have almost identical J_1, and the difference of J_2 or J_3 between the two methods is very small; (ii) method 6 has the highest J_1-J_3 values. The first phenomenon (i) can be attributed to the continually improved stability caused by PI control. The reason for (ii) is that the combination of the higher-order feedforward controller and PI feedback control overcompensates the measured displacement. In addition, methods 4-6 have lower J_1-J_3 values. This can be attributed to the fact that PI feedback control can re-compensate the measured displacement compensated by the feedforward controller, further improving the control accuracy and tracking performance of the MAC-KF method.

To present the differences between methods 1-6 in more detail, the displacement time histories of RTHS are shown in Fig. 12. The seismic excitation was El Centro, with a PGA of 0.25 g. The global and enlarged views are shown in Fig. 12(a) and Figs. 12(b) and (c), respectively. As shown in Fig. 12(a), the measured displacements were almost identical to their corresponding desired displacements, indicating excellent tracking performance of the control methods. In contrast with the results of methods 1-3 shown in Figs. 12(b) and (c), the measured displacements of methods 4-6 are better in agreement with their corresponding desired ones, demonstrating that the feedback controller is advantageous in terms of obtaining better control accuracy.

The absolute values of displacement errors for methods 1-6 are given in Fig. 13 and named errors 1-6, respectively.

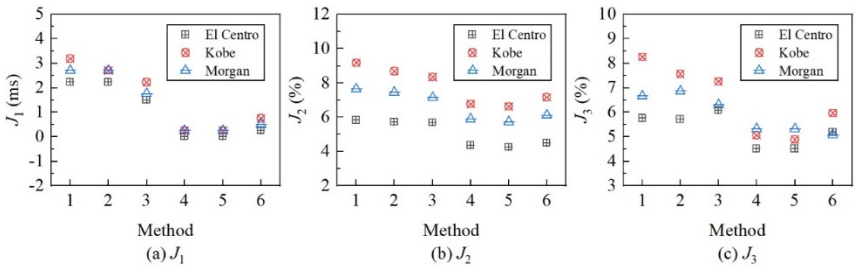

Fig. 11 J_1-J_3 of methods 1-6

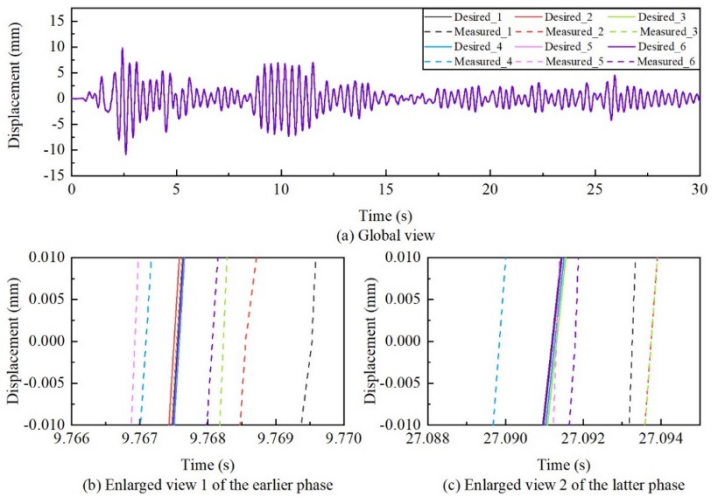

Fig. 12 Displacement time histories for methods 1-6 under El Centro with a PGA of 0.25 g

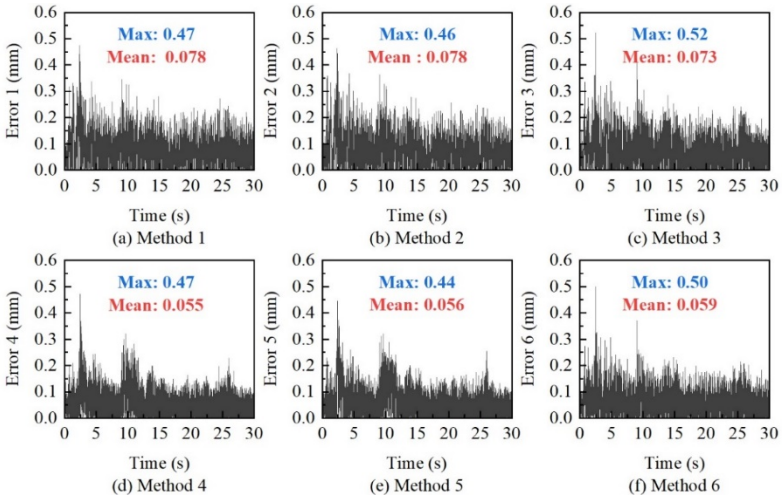

Fig. 13 Absolute values of displacement errors for methods 1-6

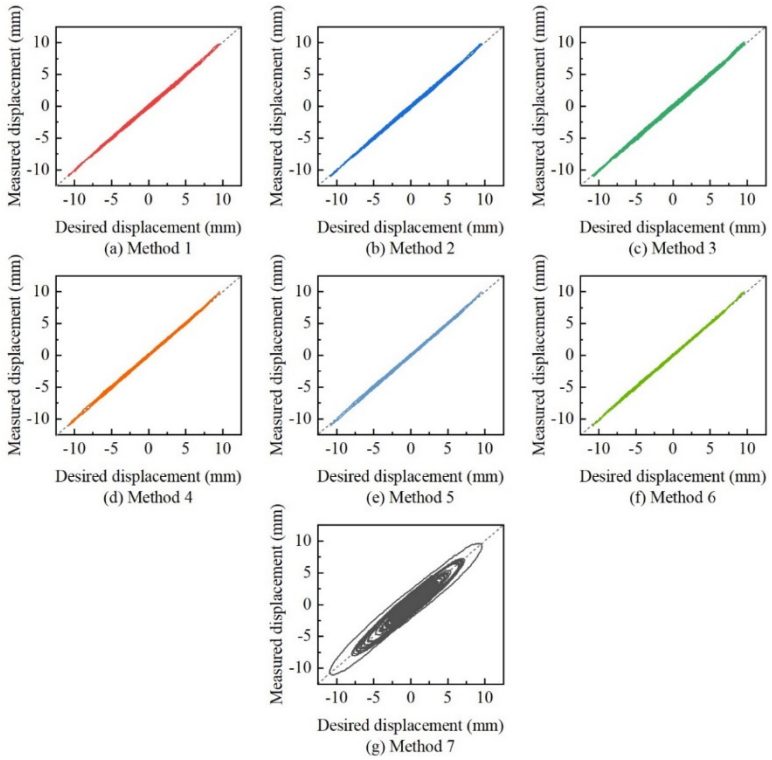

Fig. 14 Desired-measured displacement plots of methods 1-7

The "Max" and "Mean" terms in the figure denote the maximum and mean value of errors 1-6, respectively. As shown in Figs. 13(a)-(c), the trends obtained using methods 1-3 were comparable, and the "Max" and "Mean" of errors 1-3 were almost identical. A similar phenomenon can be drawn from Figs. 13(d)-(f). In addition, the maximum values of errors 4-6 were comparable to those of errors 1-3, respectively, whereas the mean values of errors 4-6 were less than those of errors 1-3. This indicates that feedback control can further improve the tracking accuracy on the basis of feedforward control.

The desired-measured displacement (D-M) relationships for methods 1-7 are shown in Fig. 14. As shown in Fig.

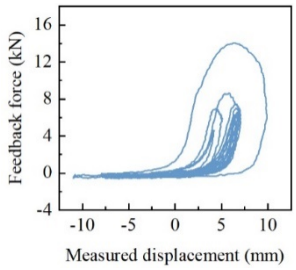

Fig. 15 Hysteresis loops of damper with method 5 under El Centro excitation

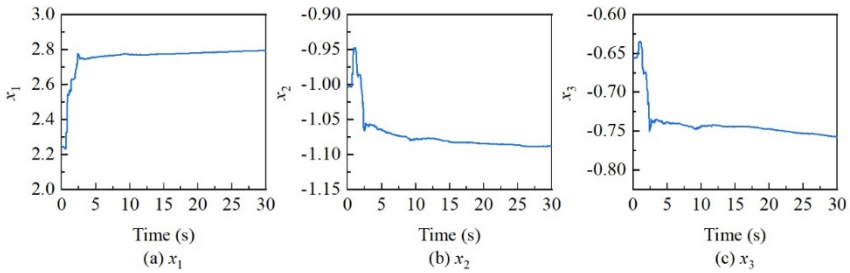

Fig. 16 Time histories of the estimated parameter for method 5 under El Centro with a PGA of 0.25 g

14(g), there were obvious discrepancies between the desired and measured displacements for method 7 owing to hysteresis loops (HLs). Meanwhile, for Figs. 14(a)-(f), the slope of the D-M relationship was almost 1, demonstrating that the de-synchronization between the NS and PS or the time delay in RTHS was decreased by the control methods. Furthermore, there are no significant differences for ADC-KFs or MAC-KFs, respectively. However, the figures show that the D-M relationships obtained using methods 4-6 were better than those obtained using methods 1-3, revealing the better control accuracy of the MAC-KF method.

The HLs of the PS for method 5 are illustrated in Fig. 15 based on the minor difference in the HLs obtained using methods 1-7. The figure shows that the damper suffered strong nonlinearity in RTHS under El Centro seismic. Nonetheless, there is extremely high synchronization between the desired and measured displacements, indicating that the ADC-KF and MAC-KF methods have excellent tracking performance. Furthermore, Figs. 13-15 show that the order of the feedforward controller has a limited effect on control accuracy and that the feedback controller is more conductive to improve the tracking performance.

Fig. 16 shows the time histories of the estimated parameter for method 5 under El Centro excitation. As shown in the figure, the parameter-updating procedure was immediately executed as RTHS began. The parameters of x_1-x_3 varied significantly from 0 s to approximately 2.5 s, and then they changed slowly. The parameters were almost comparable to their respective constants. This is almost consistent with the description in Fig. 6. The results indicate the excellent parameter identification ability of the KF.

5. Conclusions

To deal with the varying time delay in RTHS, a MAC-KF method was proposed and numerically investigated by the authors. To verify the effectiveness of the proposed MAC-KF method, this study conducted a series of validation tests for MAC-KF, including vRTHS, loading tests with a swept signal, and actual RTHSs with seismic excitations. According to the investigation results, the main conclusions are as follows:

- By comparing the RTHS results of MAC-KF with those of ADC-KF and "Bare" cases, the values of J1-J3 obtained using the MAC-KF method are the smallest, and its measured displacement best matched the desired ones, demonstrating that tracking performance can be improved to a significant extent using the proposed method.
- The results of numerical simulation and the actual experiment reveal that the order of the feedforward controller has a limited effect on the tracking performance, while the existence of feedback controller will conduce to improve the accuracy of RTHS.
- The excellent tracking performance of the MAC-KF method implies the timely and quickly adjustment of the parameters in the feedforward controller, indicating the outstanding performance of the estimation method of the KF.

Acknowledgments

The authors gratefully acknowledge the financial support provided by the National Natural Science Foundation of China [grant numbers 51908231 and 51978213], the Fundamental Research Funds for the Central Universities of Huaqiao University [grant number ZQN-912], Natural Science Foundation of Fujian Province [grant number 2020J01058], and the scientific research fund of Huaqiao University [grant number 18BS306].

References

Al-Subaihawi, S., Ricles, J.M. and Quiel, S.E. (2022), "Online explicit model updating of nonlinear viscous dampers for real time hybrid simulation", *Soil Dyn. Earthq. Eng.*, **154**, 107108. https://doi.org/10.1016/j.soildyn.2021.107108

Blakeborough, A., Williams, M.S., Darby, A.P. and Williams, D.M. (2001), "The development of real–time substructure testing", *Philosoph. Transact. Royal Soc. London. Series A: Mathe. Phys. Eng. Sci.*, **359**(1786), 1869-1891. https://doi.org/10.1098/rsta.2001.0877

Carrion, J. and Spencer, B.F. (2008), "Real-time hybrid testing using model-based delay compensation", *Smart Struct. Syst., Int. J.*, **4**(6), 809-828. https://doi.org/10.12989/sss.2008.4.6.809

Chae, Y., Kazemibidokhti, K. and Ricles, J.M. (2013), "Adaptive time series compensator for delay compensation of servo-hydraulic actuator systems for real-time hybrid simulation", *Earthq. Eng. Struct. Dyn.*, **42**(11), 1697-1715. https://doi.org/10.1002/eqe.2294

Chen, P. and Chen, P. (2020), "Robust stability analysis of real-time hybrid simulation considering system uncertainty and delay compensation", *Smart Struct. Syst., Int. J.*, **25**(6), 719-732. https://doi.org/10.12989/sss.2020.25.6.719

Chen, C. and Ricles, J.M. (2009), "Improving the inverse

compensation method for real-time hybrid simulation through a dual compensation scheme", *Earthq. Eng. Struct. Dyn.*, **38**(10), 1237-1255. https://doi.org/10.1002/eqe.904

Chen, P., Hsu, S., Zhong, Y. and Wang, S. (2019), "Real-time hybrid simulation of smart base-isolated raised floor systems for high-tech industry", *Smart Struct. Syst., Int. J.*, **23**(1), 91-106. https://doi.org/10.12989/sss.2019.23.1.091

Chen, C., Yang, Y., Hou, H., Peng, C. and Xu, W. (2022), "Real-time hybrid simulation with multi-fidelity Co-Kriging for global response prediction under structural uncertainties", *Earthq. Eng. Struct. Dyn.*, **51**(11), 2591-2609. https://doi.org/10.1002/eqe.3690

Condori, J., Maghareh, A., Orr, J., Li, H.W., Montoya, H., Dyke, S., Gill, C. and Prakash, A. (2020), "Exploiting parallel computing to control uncertain nonlinear systems in real-time", *Experim. Techniq.*, **44**(6), 735-749. https://doi.org/10.1007/s40799-020-00373-w

Darby, A.P., Williams, M.S. and Blakeborough, A. (2002), "Stability and delay compensation for real-time substructure testing", *J. Eng. Mech.*, **128**(12), 1276-1284. https://doi.org/10.1061/(ASCE)0733-9399(2002)128:12(1276)

Fermandois, G.A. and Quiroz, M. (2021), "Adaptive Compensation with Magnetorheological Dampers in RTHS Testing", *Proceedings of the 17th World Conference in Earthquake Engineering*, Sendai, Japan, September.

Gálmez, C. and Fermandois, G. (2022), "Robust adaptive model-based compensator for the real-time hybrid simulation benchmark", *Struct. Control Health Monitor.*, **29**(7). https://doi.org/10.1002/stc.2962

Gao, X., Chen, M., Chen, C. and Guo, T. (2022), "Real-time hybrid simulation with polynomial chaos NARX modeling for seismic response evaluation of structures subjected to stochastic ground motions", *J. Struct. Eng.*, **148**(9), 04022138. https://doi.org/10.1061/(ASCE)ST.1943-541X.0003451

Hakuno, M., Shidawara, M. and Hara, T. (1969), "Dynamic destructive test of a cantilever beam, controlled by an analog-computer", *Proceedings of the Japan Society of Civil Engineers*, **1969**(171), 1-9. https://doi.org/10.2208/jscej1969.1969.171_1

Hayati, S. and Song, W. (2017), "An optimal discrete-time feedforward compensator for real-time hybrid simulation", *Smart Struct. Syst., Int. J.*, **20**(4), 483-498. https://doi.org/10.12989/sss.2017.20.4.483

Horiuchi, T. and Konno, T. (2001), "A new method for compensating actuator delay in real–time hybrid experiments", *Philosoph. Transact. Royal Soc. London. Series A: Mathe. Phys. Eng. Sci.*, **359**(1786), 1893-1909. https://doi.org/10.1098/rsta.2001.0878

Horiuchi, T., Inoue, M., Konno, T. and Namita, Y. (1999), "Real-time hybrid experimental system with actuator delay compensation and its application to a piping system with energy absorber", *Earthq. Eng. Struct. Dyn.*, **28**(10), 1121-1141. https://doi.org/10.1002/(SICI)1096-9845(199910)28:10<1121::AID-EQE858>3.0.CO;2-O

Huang, L., Chen, C., Guo, T. and Chen, M.H. (2019), "Stability analysis of real-time hybrid simulation for time-varying actuator delay using the lyapunov-krasovskii functional approach", *J. Eng. Mech.*, **145**(1). https://doi.org/10.1061/(ASCE)EM.1943-7889.0001550

Li, H., Maghareh, A., Wilfredo Condori Uribe, J., Montoya, H., Dyke, S.J. and Xu, Z. (2022), "An adaptive sliding mode control system and its application to real-time hybrid simulation", *Struct. Control Health Monitor.*, **29**(1), e2851. https://doi.org/10.1002/stc.2851

Maghareh, A., Dyke, S.J., Prakash, A. and Rhoads, J.F. (2014), "Establishing a stability switch criterion for effective implementation of real-time hybrid simulation", *Smart Struct. Syst., Int. J.*, **14**(6), 1221-1245. https://doi.org/10.12989/sss.2014.14.6.1221

McCrum, D.P. and Williams, M.S. (2016), "An overview of seismic hybrid testing of engineering structures", *Eng. Struct.*, **118**, 240-261. http://dx.doi.org/10.1016/j.engstruct.2016.03.039

Mirza Hessabi, R., Ashasi-Sorkhabi, A. and Mercan, O. (2016), "A new tracking error-based adaptive controller for servo-hydraulic actuator control", *J. Vib. Control*, **22**(12), 2824-2840. https://doi.org/10.1177/1077546314548205

Mukai, Y., Yokoyama, A., Fushihara, K., Fujinaga, T. and Fujitani, H. (2020), "Real-time hybrid test using two-individual actuators to evaluate seismic performance of RC frame model controlled by AMD", *Front. Built Environ.*, **6**, 145. https://doi.org/10.3389/fbuil.2020.00145

Najafi, A. and Spencer, B.F. (2019), "Adaptive model reference control method for real-time hybrid simulation", *Mech. Syst. Signal Process.*, **132**, 183-193. https://doi.org/10.1016/j.ymssp.2019.06.023

Nakashima, M., Kato, H. and Takaoka, E. (1992), "Development of real-time pseudo dynamic testing", *Earthq. Eng. Struct. Dyn.*, **21**(1), 79-92. https://doi.org/10.1002/eqe.4290210106

Nakata, N. and Stehman, M. (2014), "Compensation techniques for experimental errors in real-time hybrid simulation using shake tables", *Smart Struct. Syst., Int. J.*, **14**(6), 1055-1079. https://doi.org/10.12989/sss.2014.14.6.1055

Ning, X., Huang, W., Xu, G., Wang, Z. and Zheng, L. (2022), "A model-based adaptive control method for real-time hybrid simulation", *Smart Struct. Syst., Int. J.*, **31**(5). [In press]

Ou, G., Ozdagli, A.I., Dyke, S.J. and Wu, B. (2015), "Robust integrated actuator control: experimental verification and real-time hybrid-simulation implementation", *Earthq. Eng. Struct. Dyn.*, **44**(3), 441-460. https://doi.org/10.1002/eqe.2479

Palacio-Betancur, A. and Gutierrez Soto, M. (2019), "Adaptive tracking control for real-time hybrid simulation of structures subjected to seismic loading", *Mech. Syst. Signal Process.*, **134**, 106345. https://doi.org/10.1016/j.ymssp.2019.106345

Peiris, L.D.H., Bartl, A., du Bois, J.L. and Plummer, A. (2020), "Passivity control with adaptive feed-forward filtering for real-time hybrid tests", *IFAC J. Syst. Control*, **12**, 100081. https://doi.org/10.1016/j.ifacsc.2020.100081

Phillips, B.M. and Spencer, B.F. (2013), "Model-based feedforward-feedback actuator control for real-time hybrid simulation", *J. Struct. Eng.*, **139**(7), 1205-1214. https://doi.org/10.1177/0959651820945515

Silva, C.E., Gomez, D., Maghareh, A., Dyke, S.J. and Spencer, B.F. (2020), "Benchmark control problem for real-time hybrid simulation", *Mech. Syst. Signal Process.*, **135**, 106381. https://doi.org/10.1016/j.ymssp.2019.106381

Simpson, T., Dertimanis, V.K. and Chatzi, E.N. (2020), "Towards data-driven real-time hybrid simulation: adaptive modeling of control plants", *Front. Built Environ.*, **6**, 570947. https://doi.org/10.3389/fbuil.2020.570947

Strano, S. and Terzo, M. (2016), "Actuator dynamics compensation for real-time hybrid simulation: an adaptive approach by means of a nonlinear estimator", *Nonlinear Dyn.* **85**(4), 2353-2368. https://doi.org/10.1007/s11071-016-2831-0

Tsokanas, N., Wagg, D. and Stojadinović, B. (2020), "Robust model predictive control for dynamics compensation in real-time hybrid simulation", *Front. Built Environ.*, **6**, 127. https://doi.org/10.3389/fbuil.2020.00127

Tsokanas, N., Zhu, X., Abbiati, G., Stefano, M., Sudret, B. and Stojadinovic, B. (2021), "A global sensitivity analysis framework for hybrid simulation with stochastic substructures", *Front. Built Environ.*, **7**, 778716. https://doi.org/10.3389/fbuil.2021.778716

Tsokanas, N., Pastorino, R. and Stojadinović, B. (2022), "Adaptive model predictive control for actuation dynamics compensation in real-time hybrid simulation", *Mech. Mach. Theory*, **172**,

104817. https://doi.org/10.1016/j.mechmachtheory.2022.104817
Wang, Z., Xu, G., Li, Q. and Wu, B. (2020), "An adaptive delay compensation method based on a discrete system model for real-time hybrid simulation", *Smart Struct. Syst., Int. J.*, **25**(5), 569-580. https://doi.org/10.12989/sss.2020.25.5.569
Weber, F. (2013), "Bouc-Wen model-based real-time force tracking scheme for MR dampers", *Smart Mater. Struct.*, **22**(4), 45012. https://doi.org/10.1088/0964-1726/22/4/045012
Xu, W., Chen, C., Gao, X., Chen, M., Guo, T. and Peng, C. (2022), "Data-driven nonlinear autoregressive with external input model-based compensation for real-time testing", *Struct. Control Health Monitor.*, **29**(12), e3119. https://doi.org/10.1002/stc.3119
Zhao, J., French, C., Shield, C. and Posbergh, T. (2003), "Considerations for the development of real-time dynamic testing using servo-hydraulic actuation", *Earthq. Eng. Struct. Dyn.*, **32**(11), 1773-1794. https://doi.org/10.1002/eqe.301
Zhao, J., Shield, C., French, C. and Posbergh, T. (2005), "Nonlinear system modeling and velocity feedback compensation for effective force testing", *J. Eng. Mech.*, **131**(3), 244-253. https://doi.org/10.1061/(ASCE)0733-9399(2005)131:3(244)

BS

Appendix 1 RTHS evaluation criteria of method 1-7 under three earthquake acceleration with the peak acceleration of 0.10 g

Number	Method	Earthquake record	J_1 (ms)	J_2 (%)	J_3 (%)
1	ADC-KF(2)	El Centro	2.90	8.37	7.62
		Kobe	4.90	13.10	11.39
		Morgan	3.90	11.03	9.25
2	ADC-KF(3)	El Centro	2.90	7.97	8.07
		Kobe	3.90	12.87	10.84
		Morgan	3.90	10.53	9.66
3	ADC-KF(4)	El Centro	2.00	7.99	7.89
		Kobe	2.90	12.01	9.22
		Morgan	2.00	9.74	7.88
4	MAC-KF(2)	El Centro	0.00	5.93	5.18
		Kobe	1.00	10.16	6.49
		Morgan	1.00	8.75	5.55
5	MAC-KF(3)	El Centro	0.00	5.62	5.27
		Kobe	1.00	9.68	6.09
		Morgan	1.00	8.21	5.38
6	MAC-KF(4)	El Centro	1.00	6.17	5.81
		Kobe	1.00	10.28	7.62
		Morgan	1.00	8.60	6.50
7	Bare	El Centro	14.60	26.75	23.56
		Kobe	14.60	26.88	24.45
		Morgan	14.60	26.31	31.23

Appendix 2 RTHS evaluation criteria of method 1-7 under three earthquake acceleration with the peak acceleration of 0.15 g

Number	Method	Earthquake record	J_1 (ms)	J_2 (%)	J_3 (%)
1	ADC-KF(2)	El Centro	2.00	5.84	5.93
		Kobe	2.90	9.60	8.50
		Morgan	2.90	7.94	6.68
2	ADC-KF(3)	El Centro	2.00	5.87	5.74
		Kobe	2.90	9.29	7.77
		Morgan	2.90	7.69	6.89
3	ADC-KF(4)	El Centro	2.00	5.86	5.90
		Kobe	2.00	8.63	7.33
		Morgan	2.00	7.37	6.08
4	MAC-KF(2)	El Centro	0.00	4.36	4.27
		Kobe	0.00	6.82	5.25
		Morgan	0.00	6.08	4.76
5	MAC-KF(3)	El Centro	0.00	4.32	4.67
		Kobe	0.00	6.88	4.89
		Morgan	0.00	5.86	4.95
6	MAC-KF(4)	El Centro	0.00	4.59	5.75
		Kobe	1.00	7.46	6.36
		Morgan	1.00	6.36	4.93
7	Bare	El Centro	13.70	25.93	23.94
		Kobe	14.60	25.71	24.17
		Morgan	13.70	25.42	31.21

Appendix 3 RTHS evaluation criteria of method 1-7 under three earthquake acceleration with the peak acceleration of 0.20 g

Number	Method	Earthquake record	J_1 (ms)	J_2 (%)	J_3 (%)
1	ADC-KF(2)	El Centro	2.00	4.86	5.03
		Kobe	2.90	7.60	7.02
		Morgan	2.00	6.27	5.95
2	ADC-KF(3)	El Centro	2.00	4.77	4.79
		Kobe	2.00	6.26	5.89
		Morgan	2.00	6.26	5.89
3	ADC-KF(4)	El Centro	1.00	4.73	5.64
		Kobe	2.00	6.94	6.30
		Morgan	2.00	6.15	5.62
4	MAC-KF(2)	El Centro	0.00	3.71	4.22
		Kobe	0.00	5.42	4.34
		Morgan	0.00	4.60	5.60
5	MAC-KF(3)	El Centro	0.00	3.70	3.98
		Kobe	0.00	5.35	4.39
		Morgan	0.00	4.69	5.48
6	MAC-KF(4)	El Centro	0.00	3.81	4.54
		Kobe	1.00	5.90	5.06
		Morgan	0.00	5.15	4.82
7	Bare	El Centro	13.70	26.03	31.78
		Kobe	14.60	25.67	23.97
		Morgan	13.70	25.07	31.80

Appendix 4 RTHS evaluation criteria of method 1-7 under three earthquake acceleration with the peak acceleration of 0.25 g

Number	Method	Earthquake record	J_1 (ms)	J_2 (%)	J_3 (%)
1	ADC-KF(2)	El Centro	2.00	4.19	4.40
		Kobe	2.00	6.37	6.10
		Morgan	2.00	5.27	4.75
2	ADC-KF(3)	El Centro	2.00	4.22	4.29
		Kobe	2.00	6.25	5.72
		Morgan	2.00	5.33	5.00
3	ADC-KF(4)	El Centro	1.00	4.13	4.86
		Kobe	2.00	5.78	6.18
		Morgan	1.00	5.28	5.62
4	MAC-KF(2)	El Centro	0.00	3.39	4.37
		Kobe	0.00	4.66	4.15
		Morgan	0.00	4.13	5.38
5	MAC-KF(3)	El Centro	0.00	3.41	4.13
		Kobe	0.00	4.59	4.20
		Morgan	0.00	4.13	5.48
6	MAC-KF(4)	El Centro	0.00	3.38	4.62
		Kobe	0.00	4.98	4.83
		Morgan	0.00	4.28	4.03
7	Bare	El Centro	13.70	27.38	45.10
		Kobe	13.70	25.00	23.20
		Morgan	13.70	25.82	33.26